Hierarchical model for distributed seismicity

Alejandro Tejedor*
Department of Theoretical Physics, University of Zaragoza, Zaragoza, Spain

Javier B. Gómez†
Department of Earth Sciences, University of Zaragoza, Zaragoza, Spain

Amalio F. Pacheco‡
Department of Theoretical Physics and BIFI, University of Zaragoza, Zaragoza, Spain

(Received 4 May 2010; published 30 July 2010)

A cellular automata model for the interaction between seismic faults in an extended region is presented. Faults are represented by boxes formed by a different number of sites and located in the nodes of a fractal tree. Both the distribution of box sizes and the interaction between them is assumed to be hierarchical. Load particles are randomly added to the system, simulating the action of external tectonic forces. These particles fill the sites of the boxes progressively. When a box is full it topples, some of the particles are redistributed to other boxes and some of them are lost. A box relaxation simulates the occurrence of an earthquake in the region. The particle redistributions mostly occur upwards (to larger faults) and downwards (to smaller faults) in the hierarchy producing new relaxations. A simple and efficient bookkeeping of the information allows the running of systems with more than fifty million faults. This model is consistent with the definition of magnitude, i.e., earthquakes of magnitude m take place in boxes with a number of sites ten times bigger than those boxes responsible for earthquakes with a magnitude $m-1$ which are placed in the immediate lower level of the hierarchy. The three parameters of the model have a geometrical nature: the height or number of levels of the fractal tree, the coordination of the tree and the ratio of areas between boxes in two consecutive levels. Besides reproducing several seismicity properties and regularities, this model is used to test the performance of some precursory patterns.

DOI: 10.1103/PhysRevE.82.016118 PACS number(s): 05.65.+b, 91.30.Dk, 91.30.pd

I. INTRODUCTION

Seismicity (either regional or single fault-related) is not prone to regularities, at least to deterministic regularities. Because of the short period of instrumental earthquake records, the statistics of naturally occurring earthquakes are poor. This fact justifies the development of "synthetic seismicity" models [1], in which long catalogs of events are generated by computer models of seismogenesis. Such models can be tuned by making them reproduce what is known of the statistics of past seismicity to a reasonable degree, and then used to make inferences about the behavior of seismicity by making use of much longer and more homogeneous catalogs of synthetic events.

Of all the statistical regularities of regional or global seismicity, the Gutenberg-Richter (GR) law is, together with the Omori law, one of the most robust. Expressed in term of the broken area of the fault, the GR law says that the number of earthquakes breaking an area bigger than A scales as a power law

$$N(>A) \propto A^{-b}, \tag{1}$$

where b is the so-called b value which, although around 1 in most cases, can fluctuate above and below this value [2,3].

Although the robustness of the GR law for regional seismicity is not questioned in the literature, the origin of this power law is not so clear. Two types of models can explain this distribution [4]. The first assumes that there is a power-law distribution of faults and each fault has its own characteristic earthquake. The second assumes that each fault has a power-law distribution of earthquakes. Observations and models in favor of and against both hypotheses are plentiful [5–14], though the first hypothesis has more experimental backup.

Evidences of power-law distributions of faults (and fractures) have been provided in a huge range of scales, from millimeters to hundreds of kilometers [15]. compiled a comprehensive review of most of them. They give ample proof that most fracture systems obey the relationship

$$dN(l) \propto l^{-a} dl, \tag{2}$$

where $dN(l)$ is the number of fracture lengths that belong to the interval $[l, l+dl]$, with $dl \ll l$, and a is the fracture-length exponent. For faults with linear sizes bigger than 100 m, the fracture-length exponent estimated from two-dimensional (2D) exposures and maps is in the range 0.8–3.5, with 70% of the data sets between 1.7 and 2.75 [15]. We will call this exponent a_{FL}^{2D}, where FL stands for fracture length as measured in 2D sections.

An alternative way of approaching the size-frequency relationship of faults is through the fractal theory of fragmentation [16–19]. Each fragment (blocks in three dimensions) is limited by surfaces that are the expression of the fractures

*atejedor@unizar.es
†jgomez@unizar.es
‡amalio@unizar.es

created in the original unbroken material during the process of fragmentation. So, by estimating the size-frequency distribution of fragments in terms of their linear dimension l, the size-frequency distribution of fractures is also being estimated. If we accept that this theory of fragmentation is not only valid at small scales but also at crustal scales [17,19], the exponent of the size-frequency distribution of fracture lengths and the exponent of the size-frequency distribution of fragment sizes (when expressed in terms of a linear dimension l) must agree. Most experiments and models of fragmentation are compatible with a power-law function of the form $N(>l) \propto l^{-D}$, where $N(>l)$ is the number of fragments with a linear dimension greater than l and D is the fractal exponent of the distribution. For three-dimensional fragmentation D is most commonly between 2 and 3 [17,20], with values of $D \approx 2.6$ favored by many experiments and models, in particular by comminution models where fracture probability is maximum for neighboring fragments of the same size, which evolve toward a geometry where no two fragments of the same size are in contact at any scale [18,19,21]. These specific models are most relevant to the type of constrained loading that affects the Earth's crust.

As written, exponent D is for a cumulative power-law distribution of fragment sizes, while exponent a_{FL}^{2D} is for a noncumulative power law of fracture lengths. So, the fractal exponent in noncumulative form will be $a_{Fr}^{3D}=D+1$, with a range $3 \leq a_{Fr}^{3D} \leq 4$ and a most probable value of $a_{Fr}^{3D} \approx 3.6$. Writing the exponent as a_{Fr}^{3D} stresses the idea that the exponent has been obtained from three-dimensional (3D) fragments (Fr) of linear size l.

How can a_{FL}^{2D} and a_{Fr}^{3D} be compared? For fracture systems with independent and homogeneous geometric parameters the transition from 2D to 3D is simply reflected by adding 1 to the exponent [5,22]: $a_{FL}^{3D}=a_{FL}^{2D}+1$. When these assumptions are not met [23], have shown that $a_{FL}^{3D}=a_{FL}^{2D}+B$, with $0 \leq B \leq 1$. Thus, to compare the ranges of a_{FL}^{2D} with those of a_{Fr}^{3D}, two end-member models can be used, namely $B=0$ and $B=1$. For $B=0$, we have $1.7 \leq a_{FL}^{3D} \leq 2.75$ (for 70% of the data sets); and for $B=1$ we have $2.7 \leq a_{FL}^{3D} \leq 3.75$ (for 70% of the data sets). Only this second model is compatible with the range $3 \leq a_{Fr}^{3D} \leq 4$ of the fractal fragmentation theory. In this case ($B=1$) the common range for both exponents is $3 \leq a^{3D} \leq 3.75$, where the subscript has been dropped to stress that the only assumption left is the three-dimensional nature of the objects. A very similar range was given by [24] following a different line of reasoning. Also [25], suggest that $a^{3D}=3$ is an attractor in the dynamics of fault systems, which in early stages of development have $a^{3D}>3$ and tend to $a^{3D}=3$ in more mature stages.

In summary, there is ample evidence that faults (and/or blocks separated by faults) have a power-law distribution of sizes. If we join this evidence with the characteristic earthquake hypothesis (i.e., each fault can produce earthquakes of just one size that corresponds to its area [26]), the GR law is an obvious outcome. And if the comminution model is also taken into account [18,19,21], the picture emerges of a set of blocks with a power-law distribution of sizes and no two blocks of the same size in contact at any scale. In this paper, we will adhere to this point of view and will implement it by means of a hierarchical model, the hierarchical box model (HBM).

The HBM is hierarchical in two ways: in the way the load is redistributed and in the positioning of the boxes (faults) according to their size. Faults in our model have a size which depends on the level of the hierarchy and, as already mentioned, can produce earthquakes of only that size. The hierarchy is implemented in the form of a fractal tree of N levels and a coordination number c.

The model that we propose here is not the first one to have a hierarchical structure. In the seismological literature the first use of a hierarchical structure can be traced back to the work of [27–30]. In the first two papers the hierarchy is implemented in the solving stage of the model, which is carried out by means of a renormalization group approach [31], and the aim was to predict the "sound" to "broken" transition in rocks. This line of thought was pursued by [32–35], who built several models where the hierarchy was implemented through the size of the blocks (or defects) that made the transition from sound to broken, differing in the rules that decide when a block/defect in one level of the hierarchy breaks as a result of the "weakness" of the blocks/defects connected to it in the lower level of the hierarchy. The paper by [34] is most interesting as the authors introduce for the first time a healing parameter, later incorporated by [36] in the colliding cascades model.

The paper by [29] was intended to explain the stick/slip transition that causes earthquakes. In this model all the elements have the same size (they can be considered as small rupture elements) and what is hierarchically organized is the way load is transferred from a failing element to other sound elements in the system. Related to this seminal work and gathered under the umbrella of fiber-bundle models, several hierarchical fracture models were later proposed [37–44] sharing with the original one the way load was hierarchically transferred between elements following the structure of a low-coordination fractal tree. Hierarchical trees also emerge in the discrete scale invariance put forward by [45] for complex systems.

Barriere and Turcotte [46] proposed a novel cellular automaton to reproduce regional seismicity in an area occupied by a large number of faults. The model represents the fault system by a grid of sites (or boxes) with a power-law distribution of sizes. Tectonic load is modeled by the addition of external load particles, and the probability of each site receiving a new particle is directly proportional to its size (area). Each site has a load threshold equal to four times its area and when the load surpasses that threshold a relaxation (earthquake) occurs. The model is economical in parameters (just two) and is able to reproduce power-law statistics for the size distribution of earthquakes. However, the b values of these distributions are not realistic. Contrary to the fiber-bundle type models, the hierarchy in Barriere and Turcotte's model applies to the distribution of fault sizes, not to the load transfer mechanism.

The final model to be mentioned here is the so-called colliding cascades model [36,47–50]. The original colliding cascades model [36] is a continuous time, continuous load model whose dynamics is based on a set of coupled ordinary differential equations. Its geometry is hierarchical, consisting of several levels, each of which is composed of several elements. The number of elements grows downwards according

to a geometric series of ratio 3 (coordination number of the fractal tree) and the top level has just one element. All elements are the same size, irrespective of the level in the hierarchy. Load is introduced in the model only through the top element and diffuses downwards. Failures can start only in the lower-most level and then travel upwards in the hierarchy. The interaction between the descending load cascade and the ascending failure cascade gives its name to the model. The size (magnitude) of an earthquake is equal to the highest level element broken in a failure avalanche.

The Colliding Cascades Model aims to reproduce the seismicity in a large area by using a hierarchical structure of block sizes. It is not economical in parameters (12 are defined in [36]) and they must be finely tuned to obtain a specific seismicity regime (the model is not self-organized critical). Also, the size-frequency relation obtained in the intermediate regime (the only one with a power-law distribution) has an unrealistic b value. In spite of these disadvantages the Colliding Cascades model is a compulsory reference within the hierarchical models of regional seismicity and has partly served to inspire us to devise the model presented here.

This paper is organized as follows: Section II presents the HBM as a pure cellular automaton, its structure, elements and its rules of updating. The correspondence between the elements of the HBM and a real network of seismic faults in a large region is detailed in Sec. III. In Sec. IV the form of fixing or bounding the three parameters of the model in order to agree with various basic elements of seismicity is indicated. Two new ingredients are commented on which are introduced to relax a little the rigidity of the pure cellular automaton. Once the parameters are fixed, in Sec. V we perform simulations of the HBM and explore the synthetic seismicity that emerges from it. Section VI contains the basic ingredients for the forecasting of the main synthetic earthquakes of the system. Section VII is dedicated to a general discussion, including the analysis of a new more physical pattern of forecasting. Finally, Sec. VIII offers our conclusions.

II. HIERARCHICAL CELLULAR AUTOMATA

The cellular automata model [51] consists of a grid of cells, each cell in one of a number of finite states. Each cell state is updated in discrete time steps according to a set of rules. These rules depend on the state of the cell and its nearest neighbors in previous or present time steps.

In this model, the grid is a fractal tree and the cells (boxes) are positioned on its nodes. The tree has N levels, which are labeled by the integer index m. A fractal tree with $N=3$ is shown in Fig. 1. The role of the boxes is to accumulate particles up to a maximum occupancy C, called its capacity, and when the occupancy reaches or exceeds C, the box relaxes and becomes empty by transferring all the particles to other boxes. Thus, each box has C sites susceptible to be occupied and therefore the possible states of occupation of a box are $0,1,2,\ldots,C-1$.

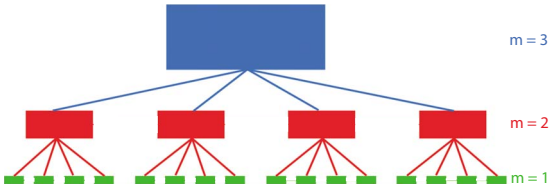

FIG. 1. (Color online) Schematic representation of the hierarchical structure used in the model. In this example the number of levels is $N=3$ and the coordination index $c=4$. The faults (boxes) are the rectangles located on the nodes of the fractal tree, while the links are the load transfer trajectories. Each level is identified by an integer m, starting from the lowest level.

The capacity of a box depends on m in the form

$$C(m) = r^{m-1}, \tag{3}$$

where r is a constant to be fixed.

Now, the coordination of the tree, or branching index, will be denoted by c (in Fig. 1, $c=4$). Due to the geometry of the system, colloquially speaking let us say that each box has one parent, c children, and $c-1$ siblings. In the strict hierarchical structure there are no links between a box and its siblings.

The geometric structure of the model is now fixed. Turning to the rules for updating the boxes, these rules are similar to those used by [52] in the Sand-Pile and in other models.

(1) At each basic time unit, one new particle is randomly added to the system from outside. The probability of any box in the system receiving this new particle is proportional to its capacity. After deciding which specific box will receive the particle, we examine whether this addition completes its capacity or not. If it does, then the box topples, otherwise, the state of the box is increased by one unit and after another time unit a new particle is added to the system. Only when toppling stops (i.e., the occupancy of all the boxes is lower than their respective C) is a new particle added to the system.

(2) Whenever a box topples, $C/2$ of the particles are transferred upwards to its parent and $C/2$ are transferred downwards to its children. On these occasions, all the c children receive the same number of particles and any remaining particle from the square repartition is randomly assigned to the children. When, as a result of a toppling, a box receives a bunch of particles, we proceed as in rule 1, assessing whether this addition exceeds its C or not. If it does, the box topples, C particles are transferred, and the rest are dissipated; otherwise, the occupancy of that box is increased by the number of added particles.

Two particular cases of rule 2 are the topplings of the boxes at $m=1$ and the box at $m=N$. In the case $m=1$, the particles transferred downwards are lost. Likewise, in the relaxation of the highest box ($m=N$) the particles transferred upwards are also lost. Together with that mentioned above, this is the dissipation mechanism used by this hierarchical system to get rid of particles and maintain a mean value of the global occupancy.

Summarizing, the parameters of this model are N, c, and r. And, as in all the models of this type, we assume the time taken by the relaxations of boxes to be very short in com-

parison with the basic time interval between the arrival of the external particles [51]. This HBM will likely arouse interest for describing other phenomena, but here we use it to model the statistical properties of seismicity over a large region.

III. HBM AS A MODEL OF EXTENDED SEISMICITY

The hierarchical model described in Sec. II is used here to simulate extended seismicity. For this propose, the boxes of the model represent the faults that exist in a region, and their relaxations correspond to earthquakes. Assuming the hypothesis of the characteristic earthquake [26], the relaxation of a box produces an earthquake of a unique magnitude, and this depends only on the level at which the fault (box) is placed.

In the description of the cellular automaton, three parameters have arisen: the constant (r) in the definition of the capacity [Eq. (3)], the number of levels in the hierarchy, N, and the coordination number, c. In the pure model, these are completely free parameters. However, from the point of view of the application of the model to seismicity, these parameters acquire a meaning and therefore their variation ranges may be restricted. They will thus be analyzed one by one.

(i) Parameter r appears in the definition of the capacity of a box which is given by Eq. (3). It is the ratio of areas between boxes placed in two consecutive levels. According to the definition of magnitude in Seismology ($m \propto \log_{10} A$, m being the magnitude of an earthquake and A the broken area) [53,54], the value of this ratio depends on the difference in magnitude corresponding to a change of one level in the model. For simplicity, a difference of *one* unit of magnitude per level has been used. In other words, the relaxation of a box produces an earthquake of magnitude m, m being the level of the box in the hierarchical structure. It is also assumed implicitly that earthquakes occurring at the first level of the hierarchy have a magnitude $m=1$. In this scenario, the value of the parameter r becomes fixed at $r=10$.

(ii) Parameter N is the number of levels in the hierarchy. It is related to the largest earthquake that is expected in a specific region. So, this parameter is fixed as soon as the studied area is selected. In this paper, $N=7$ is used in all the simulations performed, assuming therefore the largest earthquake to have a magnitude $m=7$.

(iii) Parameter c, the coordination number, is an integer representing the number of faults of a level related in the hierarchy to one fault of the next higher level. This relation has been studied in real fault systems as mentioned in the Introduction, and Sec. IV will be dedicated to analyzing how the known data from these studies restricts the range of variation of this parameter.

Apart from the geometrical parameters, the dynamic processes of the automaton can also be recast in the language of seismicity: the external loading process responsible for the random filling of the boxes (faults) simulates the remote tectonic stress in the modeled region; the relaxation of a box corresponds to an earthquake; and earthquakes are accompanied by the redistribution and dissipation of stress.

Besides the above-mentioned correspondences, there are some rules regarding the pure model described in Sec. II that can be slackened to obtain a less rigid and more realistic seismicity model. For example, in some simulations we have also considered the possibility that the relaxation of a fault occurs when it is sufficiently loaded but not necessarily full, i.e., that its occupancy on failure is, for example, 90% of its capacity and not necessarily 100%. The effect of this change is only a slight reduction in the length of the simulations, but the differences in the results are negligible, so this modification has not been implemented.

Another modification is to consider that in the process of redistribution of the load in the relaxation of a fault, a part of this load is transferred horizontally, that is, to faults of the same size. This mechanism of "horizontal" load transfer in the model would simulate stress redistribution in faults of similar size. Thus, the real number s, $0 \leq s \leq 1$, will be the fraction of the load that is transferred to its two nearest siblings (a similar parameter is introduced in the colliding cascades model [36]). This parameter, s, is assumed to be small, because this modification is only introduced as a slight perturbation of the hierarchical structure which commands the dynamics of the system. In fact, in all the results shown in this paper we have used $s=0.1$ (In Fig. 1, although not depicted, it is assumed that the set of children of a same parent are cyclically connected to each other, which implies that each box has two nearest siblings for the horizontal transfers).

Finally, because the number of faults in a tree of N levels is $(c^N-1)/(c-1)$ (e.g., in systems with $N=7$ and $c=10$, 17, and 20 this amounts to 1.1×10^6, 25.6×10^6 and 67×10^6 faults respectively), and the state of the system is specified by giving the state of all the faults (boxes), a simple and efficient bookkeeping mechanism of information has been implemented: the load is expressed as a fraction of the capacity and is implemented with a counter, a real number in the range [0, 1] (the number of occupied sites divided by the capacity), for each fault. In this way simulation times are kept reasonably low.

The simultaneous operation of all the rules and modifications mentioned in Secs. II and III (external loading, load redistribution, and dissipation) makes the model self-organized critical. This can best be shown by plotting the degree of occupancy of the model against time (the degree of occupancy of the system, or total load, is the sum of the box occupancies). Figure 2 gives the time evolution of load in a system with seven levels ($N=7$), and a coordination index of $c=20$. Figure 2(a) shows the time evolution of the total load on the system, whereas Fig. 2(b) shows the comparative load evolution in the seventh and sixth levels and the whole system, once the system is in a statistically steady state. Note in Fig. 2(a) that after a sufficiently long period of time, no matter what the initial condition for the load was, the global occupancy oscillates around a mean value of 0.51. This property, together with power laws for the size-frequency distributions of the relaxations, constitutes one of the requirements of any critically self organized model [55]. In Fig. 2(b) it is apparent that the occurrence of earthquakes of magnitude $m=7$ has a great impact on the occupancy of the $m=6$ level but not on the occupancy of the whole system. Besides, when an $m=7$ earthquake occurs, particles transferred downwards to the $m=6$ level can be transferred upwards again to level 7, all in the same time unit. For this reason, in Fig. 2(b)

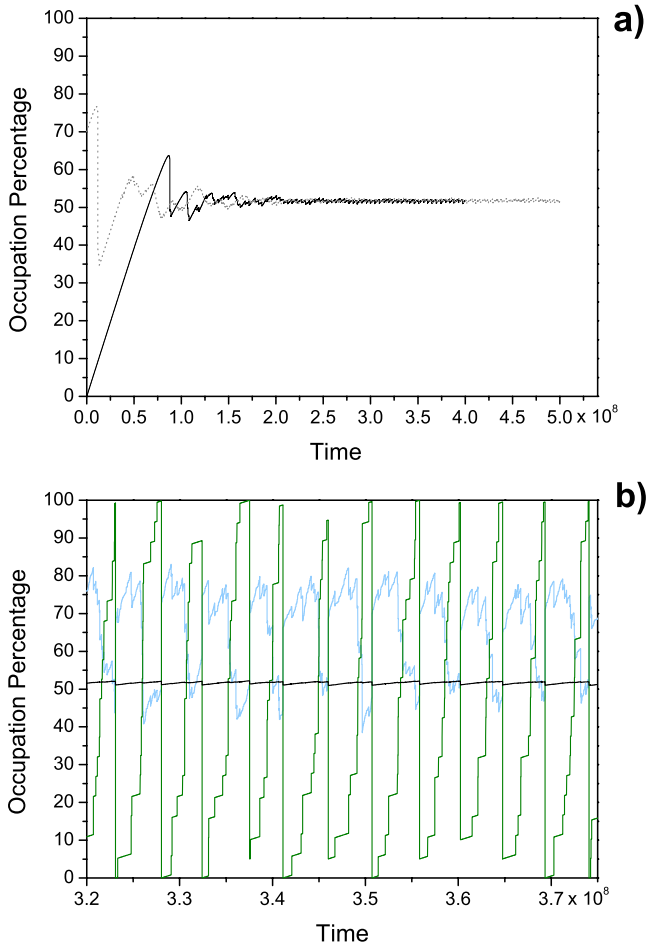

FIG. 2. (Color online) Evolution of the amount of load (total occupancy) in the system ($N=7$; $c=20$; $r=10$). (a) Evolution in the whole system. Dashed and solid lines represent a system that is initially loaded at 70% of its capacity and completely empty, respectively. (b) Comparative evolution in the seventh (green/gray line) and sixth (blue/light gray line) levels and in the whole system-black line.

the seventh level is not always empty after the occurrence of an $m=7$ earthquake.

IV. MATCHING THE MODEL WITH NATURAL SEISMICITY

As explained in the previous section, the coordination index, c, of the hierarchical structure in the model is related to the ratio of small to large faults in a region: in the model each fault in a level is directly connected to c other smaller faults in the immediate lower level. So, the first constraint on the coordination index comes naturally from the fracture length exponent. In Sec. I fracture length exponents in the range $3 \leq a \leq 3.75$ were proposed as compatible both with the size distribution of fractures in 2D sections and with the 3D size distribution of fragments in a fractal model of fragmentation. Also, the particular value $a=3.6$ was considered important following several lines of reasoning.

In the HBM, the number of boxes in each level is given by $N(m)=c^{N-m}$. Besides, the magnitude of an earthquake, m, is defined as $m=\log_{10} A+1$ (e.g., a relaxation of a box whose area is $A=10$, produces and earthquake of magnitude $m=2$). Then, the number of boxes with area A is $N(A)=c^{N+1}\cdot c^{-\log_{10} A}$. This relation can be expressed as a power law in A: $N(A)=c^{N-1}\cdot A^{-1/\log_c 10}$. And, in the continuum limit:

$$dN(A) = \frac{-1}{\log_c 10} c^{N-1} \cdot A^{-1/\log_c 10 - 1} dA. \tag{4}$$

Assuming that the characteristic length of a fault, l, is proportional to the square root of its area, then Eq. (4) becomes:

$$dN(l) \propto l^{-2/\log_c 10 - 1} dl. \tag{5}$$

Comparing this expression with Eq. (2), we conclude that $a=\frac{-2}{\log_c 10}-1$. Therefore, the coordination number of the tree can be expressed in terms of a as:

$$c = 10^{a-1/2}. \tag{6}$$

For the lower range value $a=3$, we have $c=10$; for $a=3.77$ (upper limit) we have $c=24$; and for $a=3.6$ (preferred value) we have $c=20$. So, coordination indices between 10 and 24 are compatible with the size-frequency distribution of fault sizes in the Earth's crust. Remember that r has been already fixed at $r=10$ to be consistent with the definition of seismic magnitude and with the fact that the model has a difference of one magnitude per level; likewise, N should be fixed depending on the largest earthquake expected in the studied region. This fixes or brackets the three parameters of the model.

V. SYNTHETIC SEISMICITY OF THE HBM

Notwithstanding the general lack of "premonitory" observables and deterministic regularities of regional seismicity, there are several statistical regularities that should be reproduced by any model of seismicity. In this section, we have analyzed the results that emerge from the HBM for three important regularities: GR law and b-value, the fraction of aftershocks, and the energy release rate.

(1) Gutenberg-Richter law and b-value An important check on the validity of the model is the fulfillment of the GR law. This law has two characteristics: a power-law relation between frequency and size, and an exponent of -1. Figure 3 shows the size-frequency relationship in terms of seismic magnitude for four values of the coordination number. It can be seen that the size-frequency relationship is of the GR type and that the b value is also realistic, very close to one.

(2) The fraction of triggered events (aftershocks). The next regularity of regional seismicity which is checked in our model is the fraction of aftershocks in a seismic catalog. In our model, after the addition of a new particle of load into the system, three different outcomes can be expected: (i) nothing, if the receiver box does not exceed its capacity; (ii) a single earthquake, when that box surpasses its capacity and upon load transfer no other box does; and (iii) a sequence of consecutive earthquakes when the first relaxation produces more relaxations as a consequence of the transfer of load. In

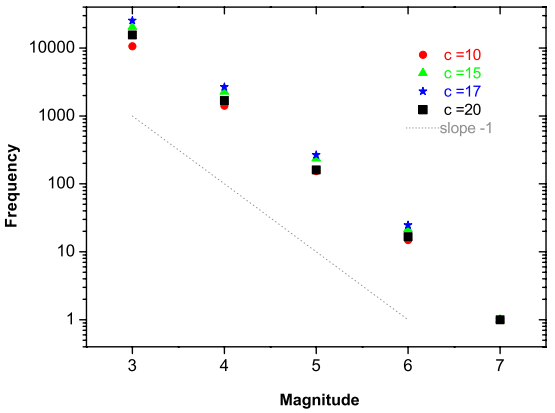

FIG. 3. (Color online) Magnitude-frequency distributions of relaxations in the HBM for $N=7$, $r=10$ and different values of c. A dotted line with slope equal to -1 has also been plotted.

the second outcome the lone earthquake is a main shock (which lacks aftershocks). In the third outcome the mainshock is identified with the biggest fault (highest level) that has relaxed in the sequence. The other relaxations are defined as aftershocks, and the number of them is registered for the statistics. Thus, due to the time-scale separation of cellular automata models, it is very simple in the HBM to compute the aftershocks-to-mainshocks ratio and compare it to expected values of this ratio in regional seismicity.

The percentage of aftershocks in the HBM is of 62% for a magnitude cutoff of $m=2$ (for the computation of the aftershock-to-mainshock ratio, earthquakes in the first level of the hierarchy are not included as their dynamics differ from that of the other levels). In real seismicity the exact proportion of triggered earthquakes depends on the region and, above all, the magnitude cutoff considered. Most estimates for a cutoff magnitude around $m\approx 2-3$ agree on a percentage of aftershocks between 60 and 80% [56–63]. The value obtained by the HBM, 62%, is within this range.

Table I separates the aftershock production by the magnitude of the mainshock. Mainshocks of magnitude $m=3$ have an average of 6 ± 3 aftershocks, while $m=7$ mainshocks have an average of 7577 ± 4616 aftershocks. As a comparison, the $m=7.3$ Landers earthquake produced around 17 000 aftershocks in the following 370 days. Extrapolating the number of aftershocks from an $m=7$ mainshock to an $m=7.3$ one in the HBM gives $13\,000\pm 8500$ aftershocks, which compares well with the actual estimate. The Hector Mine earthquake ($m=7.1$) produced around 6000 aftershocks

TABLE I. Number of aftershocks per mainshock of each magnitude in the HBM.

Magnitude of mainshock	Aftershocks per mainshock
3	6 ± 3
4	33 ± 18
5	214 ± 95
6	1207 ± 655
7	7677 ± 4616

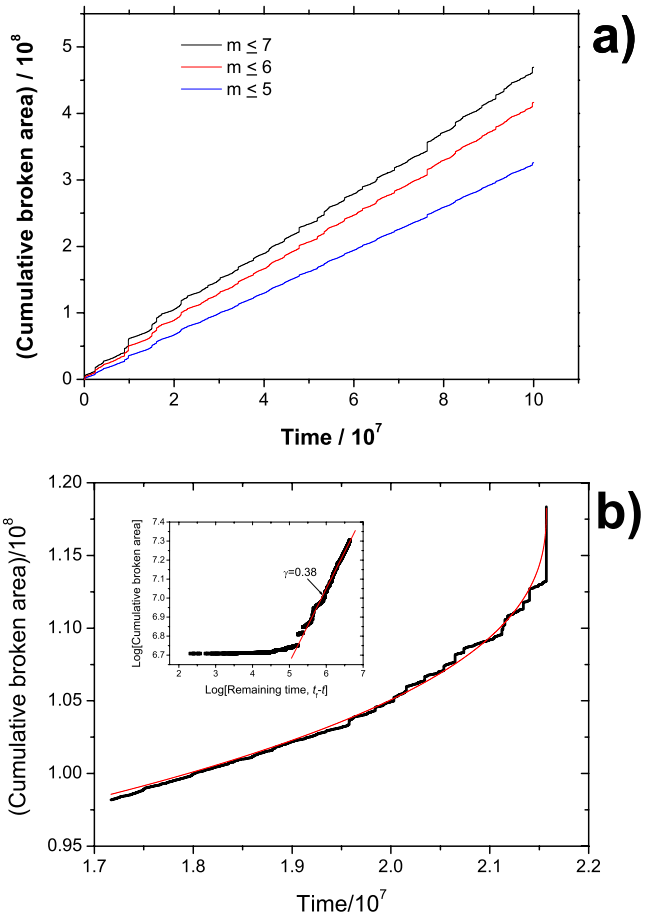

FIG. 4. (Color online) Seismic energy output of the system. (a) Accumulated long-term energy output for three different ranges of earthquakes: $m\leq 5$ (blue/lower curve), $m\leq 6$ (red/middle curve), and $m\leq 7$ (black/upper curve); this last curve is the total energy output of the system as $m=7$ earthquakes are the biggest an $N=7$ system can sustain. The total broken area is used as a proxy for the released seismic energy. (b) Short-term energy output prior to a large $m=7$ earthquake. A premonitory acceleration in the released energy following a power-law with an exponent $\gamma=0.38$ (inset) is observed.

in the first 600 days, also compatible with the HBM productivity. The $m=6.2$ Big Bear earthquake triggered around 818 aftershocks in a volume of $20\times 20\times 17$ km^3 in 375 days, while the $m=6.1$ Joshua Tree earthquake triggered around 2600 aftershocks in a volume of $20\times 20\times 19$ km^3 in 160 days [64]. In this range of magnitude (6.1–6.2) HBM's mainshocks have $1500-1800\pm 1100$ aftershocks, which also compares well with the number of aftershocks in the Joshua Tree and Big Bear earthquakes.

(3) Energy release rate. Figure 4(a) plots the energy release rate in terms of accumulated broken area (as a proxy for energy) for three earthquake size ranges, $m\leq 5$, $m\leq 6$, and $m\leq 7$. Clearly the long-term energy release rate is constant for the three magnitude ranges, although sudden steps are more evident in the $m\leq 7$ curve as a consequence of the large number of aftershocks that these large earthquakes trigger (actually, $m=7$ are the largest earthquakes that a $N=7$ system can sustain). This constant long-term energy release

rate is to be expected from a self-organized criticality (SOC) model, and also from what happens in real seismicity due to the constant long-term energy input into the crust from the dynamics of plate tectonics. However, prior to some large events [Fig. 4(b)], energy release is not constant and a premonitory acceleration in released energy can be observed. This is in agreement with many observations of accumulated Benioff strain prior to large earthquakes [65–68]. A power law fit of the form $\epsilon(t)=A+B(t_f-t)^{\gamma}$ has been suggested, with exponent $\gamma=0.26\pm0.15$ [66] when $\epsilon(t)$ is expressed in terms of the cumulative Benioff strain (the square root of the released seismic energy). Here we have obtained an exponent $\gamma=0.38$ although the comparison with real data is not direct as we have used the broken area as a proxy for the released energy.

VI. FORECASTING THE LARGE EVENTS

In addition to the statistical averages of the synthetic seismicity delivered by the HBM, it is also interesting to carry out specific studies of the largest fault in the system, i.e., that located in the Nth level of the hierarchy, particularly from the viewpoint of the predictability of the earthquakes that it generates. Thus, this section is dedicated to the predictability of the largest earthquakes in an HBM with $N=7$ levels, $c=20$ and $r=10$.

A simple way of estimating the predictability of the large earthquakes in the HBM is by means of their aperiodicity, α, also known in Statistics as the coefficient of variation. The aperiodicity is $\alpha\approx0.50$ for the recurrence of the biggest earthquake in the HBM, and this is within the range of aperiodicities estimated for real faults [13,69–72]. This value means that these large earthquakes in the system have a quasiperiodic behavior and quasiperiodicity means some predictability. Thus, the question now is: how accurately can the largest event in the model be predicted? For this enterprise we will use a graphical tool, the so-called error diagrams [73], together with specific predictive strategies [74–76].

Let us assume that one observes the occurrence of a number of $m=7$ events during a time period, T. This strategy consists of the following: after the occurrence of each event, one awaits n time units and then sets the alarm; this alarm is not cancelled until the occurrence of the next event. If the following event occurs before the alarm is set, it is counted as a prediction error. In contrast, if the next event occurs while the alarm is on, it is counted as a prediction success.

The fraction of error f_e is the number of missed events, or errors, divided by the total number of target events. Analogously, the fraction of alarm, f_a, is defined as the total time the alarm was on divided by the total time of observation, T. To evaluate the quality of any forecasting strategy in a quantitative setting, we define a loss function, L, which incorporates the trade off between the cost of missing events and the cost of keeping the alarm on. We adopt here the simplest option $L=f_e+f_a$. A poor prediction strategy leads to L values close to unity, and an ideal strategy would give $L=0$.

In the reference strategy we explore the relation between time waited to set the alarm, n, and L. There is an optimum value for n, n^*, that produces a minimum value of the loss function L, L^*. Figure 5 shows the performance of the reference strategy in an error diagram [73]. Any point on the diagonal corresponds to a value $L=1$, and this would be the result of a random prediction strategy. The irregular line shows the fraction of errors and the fraction of alarm for successive values of n. The circle on this dotted line represents the best option for the reference strategy, $L^*=0.63$ ($f_e\approx0.45; f_a\approx0.18$) corresponding to a waiting interval of $n^*=3.38\times10^6$ time units. In other words, using the reference strategy we can predict 55% of the largest earthquakes while keeping the alarm on for 18% of the time. In the Sand-Pile Model a similar analysis [77] provides a value of L^* close to unity, which was related to the early belief that SOC systems were completely unpredictable. In the next section we will try to improve on these figures using a different prediction strategy that uses additional information from seismicity.

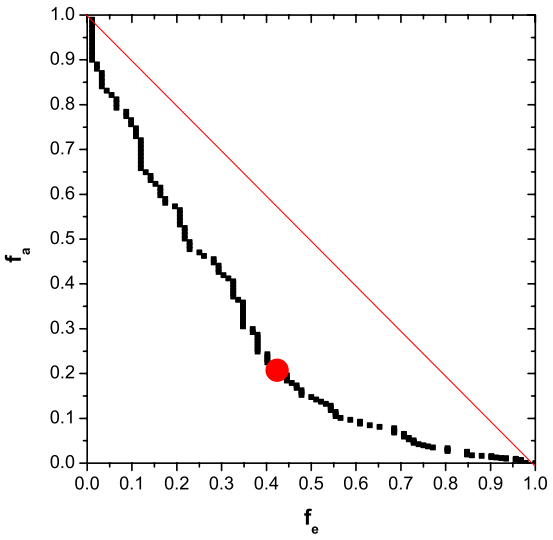

FIG. 5. (Color online) Error diagrams showing the predictability of the largest earthquake, $m=7$, in the HBM using the "reference strategy."

VII. DISCUSSION

A new cellular automaton has been presented in its generic form. Like any cellular automaton, it has very simple dynamics and a defined geometry. It has three free parameters. The interpretation of this model in terms of seismic elements, together with a little slackening of the hierarchical redistribution of load quantified by the parameter s, lead to a model for extended seismicity. With these ingredients, the HBM is able to produce synthetic catalogs of earthquakes which are compatible with some of the most important statistical regularities observed in Nature, such as the GR law, the percentage of aftershocks, the mean number of aftershocks per mainshock of magnitude m, and the rate of released energy. In spite of the fact that these successes are not sufficient to guarantee that the synthetic catalogs generated by the model are completely consistent with real seismicity, they are absolutely necessary for a synthetic catalog to be realistic.

In this section, we are going to analyze a synthetic catalog from the HBM in order to examine a regularity that has not hitherto been investigated in depth in real seismicity.

The recurrence interval of an earthquake in a specific fault is commonly assumed to be independent of fault size, though there is no reason *a priori* that this has to be the case. Following [5], if we assume that characteristic earthquakes rupture the entire length of the fault and that smaller earthquakes in the same fault have a negligible frequency, we can combine the scaling relationships for earthquakes (GR law) and faults (size-frequency relationship for fracture systems) to express the recurrence interval of earthquakes in a fault, T, in terms of the rupture length l. Mathematically the recurrence interval is the ratio of the number of faults of a given length [Eq. (2)] to the frequency of the earthquakes that take place in those faults [Eq. (1) after differentiation with the change of variable $l=A^{1/2}$]:

$$T(l) \propto \frac{l^{-a}}{l^{-2b-1}} = l^{2b-a+1}. \tag{7}$$

As b is around 1 and a varies from 3 to 3.75 as explained in Sec. I, it means that we can expect two types of behavior for the recurrence interval: (i) that it is independent of fault length ($a=3$); and (ii) that it is a decreasing function of fault length ($a>3$), although the favored value ($a=3.6$) suggests that longer faults have shorter recurrence intervals. We use the term "recurrence law" for this functional relationship between recurrence interval and fault (rupture) length.

The recurrence law can be obtained easily in our model. As the number of faults in a level m is c^{N-m} then, statistically speaking, the period of recurrence T of a fault in that level is

$$T(m) \propto \frac{c^{N-m}}{10^{-bm}}, \tag{8}$$

where m is magnitude and b the b value. The denominator in Eq. (8) is simply the GR law expressed in terms of magnitudes. Thus we have

$$T(m) \propto c^N \left(\frac{10^b}{c}\right)^m. \tag{9}$$

As $b \approx 1$, Eq. (9) implies that for $c=10$ all faults have the same recurrence interval and for $c>10$ longer faults have shorter recurrence intervals. Several simulations have been performed for $c=15$, 17, 20 to check these predictions. In these simulations one specific fault in each level was selected and its mean recurrence computed. Figure 6(a) shows the results in a plot of fault size (in terms of earthquake magnitude m) against recurrence time. Recurrence time has been normalized in each case dividing by the time of recurrence of the largest fault ($m=7$). It can be seen that the general tendency is a decrease of the time of recurrence as the size of the fault grows for the three values of the coordination number, but this tendency changes for the biggest fault in the cases of $c=15$ and $c=17$, when $m=7$ earthquakes have a slightly longer recurrence than $m=6$ ones.

Figure 6(b) examines the recurrence for an extensive compilation of active fault data from the USA [78]. Although

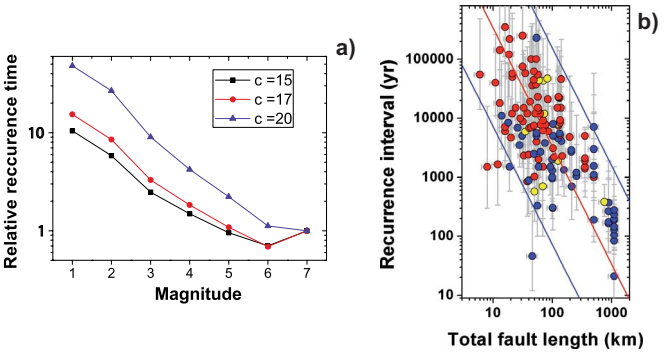

FIG. 6. (Color online) (Color Online) Recurrence law. Graph (a) recurrence intervals as a function of fault size (expressed in terms of earthquake magnitude) for three values of the coordination number: $c=15$, $c=17$, and $c=20$. (Error bars are smaller than symbols). Recurrence intervals have been scaled by the recurrence interval of the $m=7$ fault in each case. Graph (b) is a compilation of fault data (1885 faults) from the United States (USGS) for normal (red/gray), reverse (yellow/light gray), and strike-slip (blue/dark gray).

with large scatter, a negative correlation between fault length and recurrence interval is seen, compatible with the behavior of the model as shown in Fig. 6(a) ($c=20$). The result shown in Fig. 6(b) of longer faults having a shorter recurrence interval has been proposed previously [4,5], although it is by no means universally recognized [14,79]. In a recent study [14], carried out an in-depth study of six fault systems in New Zealand, USA, Greece and Italy and conclude that recurrence data (taking into account the large scatter) do not preclude a recurrence interval independent of fault length. If this is the case [see Eq. (7)], either the fracture length exponent for all the analyzed fracture systems is $a^{3D}=3$, or the assumption of each fault having a characteristic earthquake is not valid.

Although the specific recurrence law followed by real seismicity is still under debate (mainly due to the scarcity of studies and possibly to the *diversity* of recurrence laws), it seems clear that a relationship exists between the recurrence law and the fracture length exponent, and between the latter and the parameter c in the HBM.

To conclude this Section, we now explore another prediction strategy for the $m=7$ earthquakes in the HBM which is based on the observation of aftershocks [80], and which has been applied in natural seismicity. This is a type of premonitory pattern where a significant clustering of earthquakes in time is observed. It was established in intermediate-term earthquake prediction algorithms [81] and used in the colliding cascades model [47] and is one of the first premonitory seismicity patterns for which statistical significance has been established [81,82].

This prediction strategy can be applied to the HBM in the following way. Having specified the magnitude of the target earthquakes, $m=7$, we will observe all the mainshocks with magnitude $m'(m'<m)$ and the number of their respective aftershocks, $B_{m'}$. When $B_{m'}$ is equal to or bigger than a given threshold, C_B,

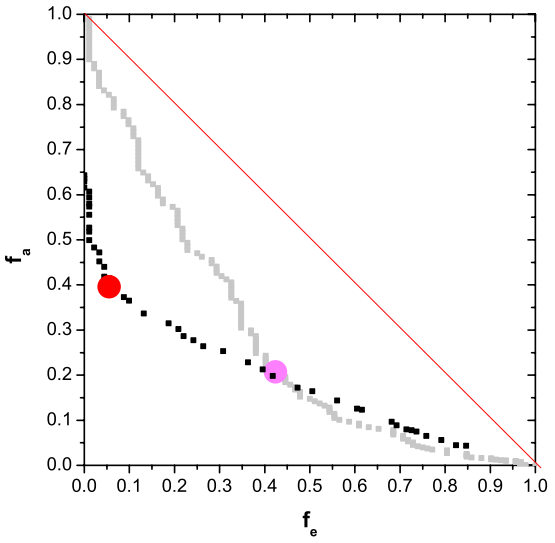

FIG. 7. (Color online) Error diagram showing the predictability of the largest earthquake, $m=7$, in the HBM using the strategy B_6. Results from the Reference Strategy (Sec. VI) are also shown (light gray) for comparison.

$$B_{m'} \geq C_B \tag{10}$$

the alarm is connected during a fixed time interval n. If an $m=7$ earthquake does not occur in this interval, the alarm is eliminated (obviously, the alarm is also immediately cancelled if the event of $m=7$ occurs). As said in Sec. VI, a prediction success is considered when the $m=7$ earthquake occurs while the alarm is on. On the other hand, it is considered an error when an event of magnitude $m=7$ occurs when the alarm is off. Thus, the two parameters to be explored in order to obtain the optimum value of $L(L^*)$ are C_B and n.

Figure 7 shows the results of carrying out this strategy where the magnitude of the mainshocks is $m'=6(B_6)$. The full circle represents the best option for this strategy, $L^*=0.45$ ($f_e=0.05$ and $f_a=0.40$) corresponding to a value of the alarm interval $n^*=2.5\times10^6$, and a number of aftershocks within the burst equal to or bigger than $C_B=2400$. Compared with the reference strategy, now 95% of the earthquakes can be predicted, although the alarm time rises to 40%.

Besides, in this strategy, in contrast with the reference strategy, there are false alarms. The fraction of false alarms, f_f, is defined as the number of times the alarm has been lifted without a prediction success, divided by the number of times the alarm has been connected. In our computation of $L^*=0.45$ its value was $f_f=0.65$.

VIII. CONCLUSIONS

The new HBM presented here to model the interaction between seismic faults in a wide region is standard in the sense that it is a cellular automata model whose elements (boxes) are located on a hierarchical scaffolding. A box receives load from the exterior and from the relaxation of its neighbors (parent, children and also from its closest siblings). When a box of the m^{th} level topples, it simulates the occurrence of an earthquake of magnitude m. This implies that in this model each fault relaxes by means of its unique characteristic earthquake. The load of the toppled box is mostly transferred up and down along the links of the hierarchical tree inducing new relaxations.

Of the new ingredients of the HBM not found in other seismicity simulators, we should stress two.

(1) The faithful representation of the logarithmic nature of the magnitude of an earthquake: boxes placed on level $m+1$ have ten times the capacity of those placed on level m.

(2) The coordination of the tree had never received any particular attention. A sort of universality had been taken for granted in the sense that the properties derived from a tree had to be similar to those derived from other trees no matter what their respective coordination, number of levels, etc. Here, we show that c is not arbitrary but is bounded by the empirical exponent of the fracture length distribution of faults and by fragmentation theory.

This model is economical in parameters. Besides the three geometrical parameters, r, N, and c, we have introduced a minor parameter s for the horizontal stress transfer. The results presented in this paper correspond to the values, $r=10$, $N=7$, $10\leq c\leq 24$, and $s=0.1$. For these values, the model is able to reproduce fundamental properties of real seismicity such as: (i) size-frequency distributions of earthquakes of the GR type with a b value equal to 1, (ii) a constant long-term rate of energy release and an accelerating short-term energy release before major earthquakes, and (iii) a number of aftershocks per mainshock of a specific magnitude, all of them in agreement with real statistics.

If the study is focused on the largest events, several results arise. The aperiodicity in the return time of the $m=7$ earthquakes is around $\alpha\approx0.50$, a reasonable value for large seismic faults [13]. There exists a tight correlation between $m=7$ and 6 events. This is natural because between these two levels there is a direct transfer of load. This fact has been used for forecasting purposes, the success of the B_6 strategy being the manifestation of the mentioned correlation. Thus, the HBM puts in evidence the fact that in spite of exhibiting a power-law behavior for the size frequency of relaxations, which is one of the genuine manifestations of the SOC systems, some important properties such as the recurrence of the largest events can be predicted with significant accuracy.

So far we have seen some of the virtues of the model. However, it does also have its shortcomings. As mentioned, this is a cellular automata model, so both time and load are discrete magnitudes. The discrete time together with the separation of temporal scales makes it impossible to establish a chronological order within an aftershock series. On the other hand, the discrete geometric structure of the hierarchical tree, c, being a constant integer, would make the representation of noninteger magnitudes difficult.

An important ingredient in most models of seismicity is *heterogeneity*. Heterogeneity has been introduced in models in many ways, affecting all possible parameters, variables or even "constants" of the models. In this sense the HBM, as presented here, is highly *homogeneous*: (i) all faults located at the same level have the same size; (ii) each fault can generate earthquakes of one specific size; (iii) all faults are directly connected to c other faults, c being a constant in each simulation; (iv) all boxes (faults) fail at the same thresh-

old load (when the occupancy is equal to its capacity); (v) the "stress drop" is equal in all faults as a box empties completely after a relaxation, etc. Most of these homogeneity constraints can be relaxed. Likewise, the symmetric option chosen for the direction of the load transfers upwards and downwards could be also relaxed. The results presented in this paper can be used as a benchmark against which the nonhomogeneous versions of the model can be assessed.

ACKNOWLEDGMENTS

We acknowledge Ilya Zaliapin and María Luisa Osete for useful comments and suggestions. Álvaro González provided Fig. 6(b). Many of the numerical simulations of this model were carried out using the computational facilities of the BIFI at the University of Zaragoza. This work was supported in part by a project of the Spanish Ministry of Science.

[1] R. Robinson and R. Benites, J. Geophys. Res. **100**, 18229 (1995).
[2] I. Main, Rev. Geophys. **34**, 433 (1996).
[3] J. F. Pacheco, C. H. Scholz, and L. R. Sykes, Nature (London) **355**, 71 (1992).
[4] D. L. Turcotte, *Fractals and Chaos in Geology and Geophysics*, 2nd ed. (Cambridge University Press, Cambridge, England, 1997).
[5] R. Marrett, Geophys. Res. Lett. **21**, 2637 (1994).
[6] S. G. Wesnousky, Bull. Seismol. Soc. Am. **84**, 1940 (1994).
[7] T. T. Cladouhos and R. Marrett, J. Struct. Geol. **18**, 281 (1996).
[8] R. B. Hofmann, Eng. Geol. (Amsterdam) **43**, 5 (1996).
[9] M. W. Stirling, S. G. Wesnousky, and K. Shimazaki, Geophys. J. Int. **124**, 833 (1996).
[10] G. Yielding, T. Needham, and H. Jones, J. Struct. Geol. **18**, 135 (1996).
[11] M. V. Matthews, W. L. Ellsworth, and P. A. Reasenberg, Bull. Seismol. Soc. Am. **92**, 2233 (2002).
[12] R. López-Ruiz, M. Vázquez-Prada, J. B. Gómez, and A. F. Pacheco, Terra Nova **16**, 116 (2004).
[13] L. R. Sykes and W. Menke, Bull. Seismol. Soc. Am. **96**, 1569 (2006).
[14] V. Mouslopoulou, J. J. Walsh, and A. Nicol, Earth Planet. Sci. Lett. **278**, 186 (2009).
[15] E. Bonnet, O. Bour, N. E. Olding, P. Davy, I. Main, P. Cowie, and B. Berkowitz, Rev. Geophys. **39**, 347 (2001).
[16] G. King, Pure Appl. Geophys. **121**, 761 (1983).
[17] D. Turcotte, Tectonophysics **132**, 261 (1986).
[18] C. G. Sammis, G. King, and R. Biegel, Pure Appl. Geophys. **125**, 777 (1987).
[19] C. G. Sammis and S. J. Steacy, in *Fractals in Earth Sciences*, edited by C. C. Barton and P. R. L. Pointe (Plenum, New York, 1995), pp. 179–204.
[20] G. Corvin, *Fractal Models in the Earth Sciences* (Elsevier Science, New York, 1992).
[21] S. J. Steacy and C. G. Sammis, Nature (London) **353**, 250 (1991).
[22] R. Marrett and R. W. Allmendinger, J. Struct. Geol. **13**, 735 (1991).
[23] H. G. Borgos, P. A. Cowie, and N. H. Dawers, J. Geophys. Res. **105**, 28,377 (2000).
[24] D. L. Turcotte and J. Huang, in *Fractals in Earth Sciences*, edited by C. C. Barton and P. R. L. Pointe (Plenum, New York, 1995), pp. 179–204.
[25] D. Sornette and P. Davy, Geophys. Res. Lett. **18**, 1079 (1991).
[26] D. P. Schwartz and K. J. Coppersmith, J. Geophys. Res. **89**, 5681 (1984).
[27] C. J. Allègre, J. L. Lé Mouel, and A. Provost, Nature (London) **297**, 47 (1982).
[28] T. R. Madden, J. Geophys. Res. **88**, 585 (1983).
[29] D. L. Turcotte, R. F. Smalley, and S. A. Solla, Nature (London) **313**, 671 (1985).
[30] R. F. Smalley, Jr., D. L. Turcotte, and S. A. Solla, J. Geophys. Res. **90**, 1894 (1985).
[31] L. Kadanoff, Physics **2**, 263 (1966).
[32] G. S. Narkunskaya and M. G. Shnirman, Phys. Earth Planet. Inter. **61**, 29 (1990).
[33] C. J. Allègre, J. Louis Le Mouël, H. Duyen Chau, and C. Narteau, Phys. Earth Planet. Inter. **92**, 215 (1995).
[34] E. M. Blanter and M. G. Shnirman, Phys. Rev. E **53**, 3408 (1996).
[35] E. M. Blanter, M. G. Shnirman, and J. L. L. Mouël, Phys. Earth Planet. Inter. **103**, 135 (1997).
[36] A. Gabrielov, V. Keilis-Borok, I. Zaliapin, and W. I. Newman, Phys. Rev. E **62**, 237 (2000).
[37] S. Pradhan, A. Hansen, and B. K. Chakrabarti, Rev. Mod. Phys. **82**, 499 (2010).
[38] W. I. Newman and A. M. Gabrielov, Int. J. Fract. **50**, 1 (1991).
[39] W. I. Newman, A. M. Gabrielov, T. A. Durand, S. L. Phoenix, and D. L. Turcotte, Physica D **77**, 200 (1994).
[40] W. I. Newman, D. L. Turcotte, and A. M. Gabrielov, Phys. Rev. E **52**, 4827 (1995).
[41] J. B. Gómez and A. F. Pacheco, Nonlinear Processes Geophys. **4**, 207 (1997).
[42] J. B. Gómez and A. F. Pacheco, Phys. Rev. E **73**, 047104 (2006).
[43] M. Vázquez-Prada, J. B. Gómez, Y. Moreno, and A. F. Pacheco, Phys. Rev. E **60**, 2581 (1999).
[44] Y. Huang, H. Saleur, C. Sammis, and D. Sornette, EPL **41**, 43 (1998).
[45] D. Sornette, Phys. Rep. **297**, 239 (1998).
[46] B. Barriere and D. L. Turcotte, Phys. Rev. E **49**, 1151 (1994).
[47] A. Gabrielov, I. Zaliapin, W. I. Newman, and V. Keilis-Borok, Geophys. J. Int. **143**, 427 (2000).
[48] I. Zaliapin, V. Keilis-Borok, and M. Ghill, J. Stat. Phys. **111**, 815 (2003).
[49] I. Zaliapin, V. Keilis-Borok, and M. Ghill, J. Stat. Phys. **111**, 839 (2003).
[50] M. Ghil, I. Zaliapin, and B. Coluzzi, Physica D **237**, 2967 (2008).
[51] B. Malamud and D. Turcotte, IEEE Comput. Sci. Eng. **2**, 42 (2000).
[52] P. Bak, C. Tang, and K. Wiesenfeld, Phys. Rev. Lett. **59**, 381

(1987).
[53] B. Gutenberg and C. F. Richter, Bull. Seismol. Soc. Am. **34**, 185 (1944).
[54] H. Kanamori and D. L. Anderson, Bull. Seismol. Soc. Am. **65**, 1073 (1975).
[55] H. J. Jensen, *Self-Organized Criticality: Emergent Complex Behavior in Physical and Biological Systems*, Lecture Notes in Physics Vol. 10 (Cambridge University Press, Cambridge, England, 1998).
[56] J. K. Gardner and L. Knopoff, Bull. Seismol. Soc. Am. **64**, 1363 (1974).
[57] S. D. Davis and C. Frohlich, J. Geophys. Res. **96**, 6335 (1991).
[58] Y. Kagan, Geophys. J. Int. **106**, 135 (1991).
[59] L. Knopoff, Proc. Natl. Acad. Sci. U.S.A. **97**, 11880 (2000).
[60] J. Zhuang, Y. Ogata, and D. Vere-Jones, J. Geophys. Res. **109**, B05301 (2004).
[61] D. Sornette and M. J. Werner, J. Geophys. Res. **110**, B08304 (2005).
[62] I. Zaliapin, A. Gabrielov, V. Keilis-Borok, and H. Wong, Phys. Rev. Lett. **101**, 018501 (2008).
[63] D. Marsan and O. Lengline, Science **319**, 1076 (2008).
[64] M. C. Robertson, C. G. Sammis, M. Sahimi, and A. J. Martin, J. Geophys. Res. **100**, 609 (1995).
[65] C. G. Bufe and D. J. Varnes, J. Geophys. Res. **98**, 9871 (1993).
[66] H. G. Bowman, G. Ouillon, C. G. Sammis, A. Sornette, and D. Sornette, J. Geophys. Res. **103**, 24359 (1998).
[67] H. G. Bowman and G. C. P. King, Geophys. Res. Lett. **28**, 4039 (2001).
[68] G. Zöller and S. Hainzl, Geophys. Res. Lett. **29**, 1558 (2002).
[69] S. P. Nishenko and R. Buland, Bull. Seismol. Soc. Am. **77**, 1382 (1987).
[70] W. L. Ellsworth, M. V. Matthews, R. M. Nadeau, S. P. Nishenko, P. A. Reasenberg, and R. W. Simpson, United States Geological Survey Open-File Report **99**, 552 (1999).
[71] A. G. Lindh, Seismol. Res. Lett. **76**, 3 (2005).
[72] T. Parsons, J. Geophys. Res. **110**, B05S02 (2005).
[73] G. M. Molchan, Pure Appl. Geophys. **149**, 233 (1997).
[74] C. G. Sammis and S. W. Smith, Pure Appl. Geophys. **155**, 307 (1999).
[75] M. Vázquez-Prada, Á. González, J. B. Gómez, and A. F. Pacheco, Nonlinear Processes Geophys. **10**, 565 (2003).
[76] V. Keilis-Bork and A. Soloviev, *Nonlinear Dynamics of the Lithosphere and Earthquake Prediction* (Springer, New York, 2003).
[77] S. L. Pepke and J. M. Carlson, Phys. Rev. E **50**, 236 (1994).
[78] A. González, J. B. Gómez, and A. F. Pacheco, Geophys. Res. Abstr. **8**, 02284 (2007).
[79] A. Nicol, J. Walsh, T. Manzocchi, and N. Morewood, J. Struct. Geol. **27**, 541 (2005).
[80] V. I. Keilis-Borok, L. Knopoff, and I. M. Rotvain, Nature (London) **283**, 259 (1980).
[81] V. I. Keilis-Borok and P. S. Shebalin, Phys. Earth Planet. Inter. **111**, 179 (1999).
[82] G. Molchan and O. Dmitrieva, Phys. Earth Planet. Inter. **61**, 99 (1990).